






Liquid-crystal based drift-free polarization modulators: Part I. Design and operation

JEAN REHBINDER,  JEAN DELLINGER, BRISÉIS VARIN,  MARC TORZYNSKI, YOSHITATE TAKAKURA, CHRISTIAN HEINRICH,  AND JIHAD ZALLAT*

Laboratoire ICube, Université de Strasbourg, Bd Sébastien Brant, 67412 Illkirch, France

*jihad.zallat@unistra.fr

Abstract: We report a new design for temperature-stable polarization modulators. Each modulator is composed of two liquid crystal variable retarders (LCVRs) positioned in such a way that their temperature drifts mutually compensate. We propose a model for the temperature-dependent polarization response of LCVRs, which permits us to establish expressions for the operating point of the system and for its accessible retardance range. We have validated such a model experimentally by thorough analyses of LCVR temperature responses, and we have built a polarization modulator that is stable over a wide range of temperature with commercially available LCVRs.

© 2022 Optica Publishing Group under the terms of the [Optica Open Access Publishing Agreement](#)

1. Introduction

Polarimetry has found use in a very wide range of applications. A common requirement is the need for precise control of light polarization. Among available technologies for modulating polarization, Liquid Crystal Variable Retarders (LCVRs) are ideal candidates for imaging polarimetry. LCVRs have several advantages as compared to other modulation techniques. They operate without moving parts, so that errors associated with mechanical rotations (e.g. alignment error [1], beam-wandering, etc.) may be avoided. Their fast switching time (down to a few milliseconds) is consistent with video-rate acquisition, and they can maintain polarization states for durations that are compatible with the integration times of CCD and CMOS cameras. LCVRs operate over a continuous range of retardance. Polarization modules based on such a technology can attain any polarization state on the Poincaré sphere. Finally, they can be fabricated in various form factors, down to very compact arrangements and, may be driven by low voltage so that very little constraints are imposed on controlling circuits.

The main drawback of LCVR-based polarization controllers is their temperature dependence. The rate of birefringence variation with temperature depends on the liquid crystal or liquid crystal mixture [2]. In general, for a given LCVR module, the absolute variation of retardance with temperature is higher at lower driving voltage [3]. In practice, temperature dependence puts stringent limits on the operating range of polarimeters built with LCVRs: thermal effects may be neglected only for variations of $\pm 1^\circ\text{C}$ [4].

In this work, we propose a new design for temperature-stable Liquid Crystal Modulator (LCM), with passive drift compensation. In section 2, we present a model for the temperature dependence of LCVRs and derive theoretical conditions for temperature stable LCM. In section 3 we detail the experimental procedures employed to characterize LCVRs and associated data analyses. Such investigations permitted us to build LCMs that are operational. Experimental validation of the proposed modulator is presented in section 4. Section 5 is devoted to discussions and conclusions.

2. Modulator design

2.1. Model for the temperature dependence of a single LCVR

The materials employed to fabricate LCVRs feature interesting physicochemical properties [5]. They are rod like molecules in a phase referred to as liquid crystal. It means that the relative positions of the molecules are not perfectly regular, while their orientations feature a long-range order. That is: their major axes tend to align along a common direction. As a result of dielectric anisotropy induced by the phase called nematic, the refractive index differs for light polarized along that direction or perpendicular to it. Such liquid crystals are birefringent. In addition, when an electric field is applied and depending on the nature of the anisotropy, the molecules would align themselves in the direction of the field, or perpendicular to it.

Taking into account such properties, LCVRs act as electrically controlled waveplates with fixed eigenaxes and continuously drivable retardance. The liquid crystal would be inserted in between two transparent electrodes, with micro-channels directing the orientation of the molecules in the absence of a voltage. The retardance of an LCVR would be maximal at 0 V, and would decrease beyond a critical voltage known as the Fréedericksz threshold voltage (for homogenous alignment of the liquid crystals); the opposite would be the case for homeotropic alignment.

Alignment of the molecules in the liquid crystal phase is not perfect. It fluctuates over time. Such fluctuations are related to the thermal energy of the molecules and increase with temperature. To quantify alignment in the liquid crystal, an order parameter noted Q has been introduced [6] and is expressed as:

$$Q = \frac{1}{2} \langle 3 \cos^2 \theta - 1 \rangle, \quad (1)$$

where θ is the angle between the major axis of each individual molecule and the common direction, with the brackets representing the ensemble average over a large number of molecules. When the molecules are perfectly aligned, Q is equal to 1 while completely random orientations would result in $Q = 0$.

Q decreases as the temperature increases in typical liquid crystals. In the absence of an electric field, the temperature dependence of the order parameter is usually determined using the Haller approximation [7]:

$$Q = Q_0 \left(1 - \frac{T}{T_C} \right)^\beta, \quad (2)$$

where β is the critical exponent and T_C is called the "clearing point", which represents the transition temperature between the nematic and the isotropic phase.

The apparent birefringence seen by the light passing through the liquid crystal is directly related to the degree of order. Randomly oriented molecules would represent a medium without birefringence while perfectly aligned molecules maximize its value. Although birefringence is not strictly proportional to Q [8], it is closely related. In fact, birefringence can be used to measure the order parameter [8] and follows the same approximation [2,3,9,10]:

$$\Delta n = \Delta n_0 \left(1 - \frac{T}{T_C} \right)^\beta. \quad (3)$$

The clearing point can vary significantly from one liquid-crystal (or liquid-crystal mixture) to another: in the works cited above, clearing points range from 307 to 386 K. In fact, this parameter is very sensitive to the molecular structure [11] and can be tailored by chemical engineering. On the contrary, the critical exponent is of the same order in most of the liquid crystals, typically around $\beta \simeq 0.2$ (β ranging from 0.1 to 0.27 in the previous reference). On a temperature range that would be small enough around a given T_0 , the expression for the temperature-dependent

retardance ϕ of a LCVR can be linearized (first-order approximation, see also Fig. S1 in Supplement 1) as:

$$\phi(T) = \phi_{T_0} + \tau \cdot (T - T_0). \quad (4)$$

In the presence of an electric field, an additional external force produces a torque on the molecules. Temperature fluctuations become less influent and the decrease of birefringence with increasing temperature occurs at a slower rate. Empirical observations confirm this intuitive explanation [9,10]. To our knowledge, this effect has not been studied theoretically. Attempts to fit Eq. (3) to temperature-dependent data result in voltage-dependent β parameter, indicating that Haller formula might not be applicable in this case [3]. A first order model can still be applied, however with a temperature dependent slope τ .

In this work, we assume that, for each voltage V , τ is proportional to the retardance at the starting temperature T_0 . Such a model can be written as:

$$\phi(T, V) = \phi_{T_0}(V) + \tau(V)(T - T_0) = \phi_{T_0}(V) + \alpha \phi_{T_0}(V)(T - T_0), \quad (5)$$

where T_0 is the expected operating temperature, and α is a coefficient characteristic of any individual LCVR.

The model is based on our own investigations (see section 4.1) as well as on indications from the manufacturer. Indeed, the data sheet of the LCVRs used in this study indicates retardance variations of approximatively -0.4% per °C, i.e. $\alpha = -0.004/^\circ\text{C}$.

2.2. Modulator design

The LCM design consists of two LCVRs positioned one behind the other with mutually orthogonal eigenaxes (see Fig. 1). We note LCVR_A the first LCVR in the optical path and LCVR_B the second one, θ_a and θ_b the orientation of their fast axis respectively to the laboratory coordinates and ϕ_a and ϕ_b their retardances.

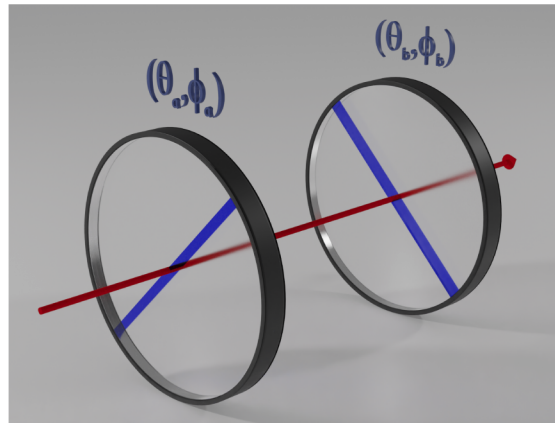


Fig. 1. LCM design. LCVR_A (resp. LCVR_B) is placed at angle θ_a (θ_b) and has a retardance ϕ_a (ϕ_b). The fast axis is represented by a blue line on each LCVR and the LCVRs are placed such that $\theta_b = \theta_a + \pi/2$. The optical axis and the direction of propagation of light are represented by the red arrow.

As stated earlier, an LCVR acts as an electrically controlled waveplate with fixed eigenaxes, and variable retardance. The polarization modulation induced by the LCVR is characterized by

its Mueller matrix M , such as:

$$M_{LCVR}(\theta, \phi) = m_{11} \begin{pmatrix} 1 & 0 & 0 & 0 \\ 0 & \cos^2(2\theta) + \sin^2(2\theta) \cos(\phi) & \sin(2\theta) \cos(2\theta)(1 - \cos(\phi)) & -\sin(2\theta) \sin(\phi) \\ 0 & \sin(2\theta) \cos(2\theta)(1 - \cos(\phi)) & \sin^2(2\theta) + \cos^2(2\theta) \cos(\phi) & \cos(2\theta) \sin(\phi) \\ 0 & \sin(2\theta) \sin(\phi) & -\cos(2\theta) \sin(\phi) & \cos(\phi) \end{pmatrix} \quad (6)$$

where m_{11} is the transmittance of the LCVR. It can be easily verified that rotating an LCVR by 90° is equivalent to changing the sign of its retardance:

$$M_{LCVR}(\theta + \frac{\pi}{2}, \phi) = M_{LCVR}(\theta, -\phi). \quad (7)$$

Finally, two waveplates with their eigenaxes aligned are equivalent to a waveplate with their retardances added. Hence, the LCM is equivalent to a single LCVR with a retardance equal to the difference individual retardances [12]:

$$M_{LCM}(\theta, \phi_a, \phi_b) = M_{LCVR}(\theta, \phi_a - \phi_b). \quad (8)$$

Temperature drift may be compensated when both LCVRs exhibit the same deviation of retardance. Additionally, if we want the LCM to maintain the same retardance over a wide range of temperature, the retardance of both LCVRs must follow a same pattern. If the drift is linear over the selected range of temperature, this is equivalent to choose a working point where the slope is the same for the LCVRs, ensuring temperature stability over the whole range.

2.3. Attainable stabilized retardance range

Based on the proposed LCM model, it is possible to establish useful expressions for temperature compensation. Working points (the choice of retardance for each LCVR) as well as attainable stabilization range for the LCM may be obtained, with only very few parameters.

If we note α_a and α_b the proportionality coefficient (as defined in Eq. (5)) for the first and the second LCVR respectively, the following relation can be easily derived:

$$\phi_a(T) - \phi_b(T) = \phi_a(T_0) - \phi_b(T_0) \iff \alpha_a \phi_a(T_0) = \alpha_b \phi_b(T_0). \quad (9)$$

Such a simple relation has several implications on the operating LCM. First, it indicates that the retardance drift can be corrected only for accurately calibrated LCVR A and B. In the case of a slope mismatch, a residual drift would remain. Another interesting observation is that identical LCVRs ($\alpha_a = \alpha_b$) do not allow correction since the condition of Eq. (9) imposes a zero retardance for the LCM. Conversely, dissimilarity in α_a and α_b is in favor of compensation, and allows higher retardance for the compensated module.

In practice, given a desired retardance ϕ_{LCM} for the LCM, it is useful to estimate ϕ_a and ϕ_b (and their corresponding driving voltages). The following simple formulas may be obtained from Eq. (9):

$$\phi_a = \phi_{LCM} \frac{\alpha_b}{\alpha_b - \alpha_a}, \phi_b = \phi_{LCM} \frac{\alpha_a}{\alpha_b - \alpha_a}. \quad (10)$$

The choice of the working points for the LCM is illustrated in Fig. 2. We have simulated the slope τ of $\phi(T)$ as a function of the retardance $\phi(T_0)$. According to the model that has been presented, τ is negative and proportional to $\phi(T_0)$. For an operation that would be temperature stable, the slope must be equal for both LCVRs. This permits to identify points that form a horizontal segment in the figure.

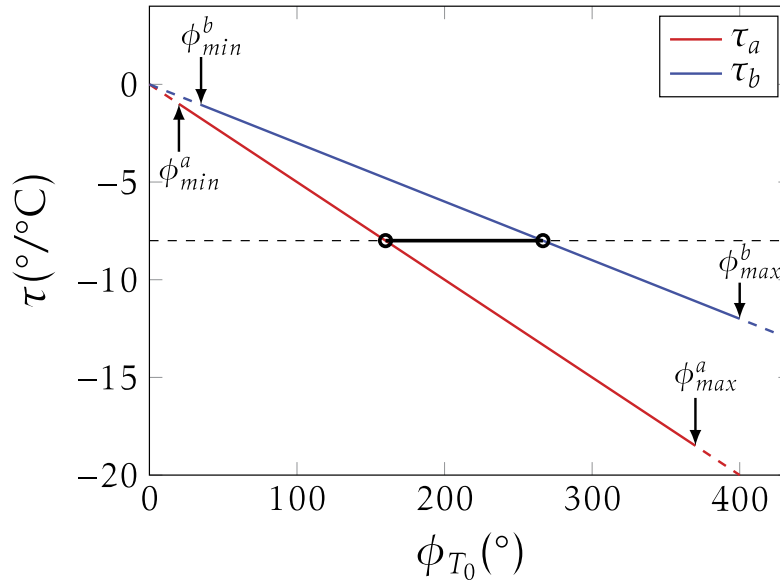


Fig. 2. Simulation illustrating the choice of working points for the LCM. The slope τ of the temperature dependence is represented as a function of the retardance at T_0 for LCVR A (blue) and LCVR B (red). Attainable values, i.e. those situated between ϕ_{min} and ϕ_{max} , are marked by a solid line. A point respecting Eq. (9) is represented by a horizontal line connecting the blue and red lines.

The following statement becomes obvious from the figure: to obtain high retardance for the LCM, it is necessary for A and B to respond with high retardances. However, LCVRs have limited ranges of accessible values. Therefore, correction of temperature dependence may be subject to restrictions.

The limiting range may be predicted with the model, by considering the minimal and maximal retardance (ϕ_{min} and ϕ_{max}) of both LCVRs:

$$\begin{aligned}\phi_{min}^{LCM} &= \max\left(\frac{\alpha_b - \alpha_a}{\alpha_b} \phi_{min}^a, \frac{\alpha_b - \alpha_a}{\alpha_a} \phi_{min}^b\right), \\ \phi_{max}^{LCM} &= \min\left(\frac{\alpha_b - \alpha_a}{\alpha_b} \phi_{max}^a, \frac{\alpha_b - \alpha_a}{\alpha_a} \phi_{max}^b\right).\end{aligned}\quad (11)$$

It is assumed here that the LCVR can only produce positive retardance, and that α_a, α_b are both negative with $|\alpha_a| < |\alpha_b|$. Similar expressions can easily be derived from Eqs. (9) and (10) for other cases.

3. Materials and methods

We will now validate our investigations and the LCM design by performing two distinct experiments. They have been set in a heated enclosure where the LCVRs were mounted so as to assess their temperature behavior. In Experiment 1, the polarimetric response of a single LCVR has been assessed. Experiment 2 has been conducted for the study of an LCM (combining two LCVRs), more precisely devoted to working points of temperature-stable operations.

3.1. Optical setup

The optical setup for Experiment 1 is detailed in Fig. 3. A commercially available LCVR (Meadowlark, LRC 300 VIS) is introduced in a heated enclosure. The latter is thermally isolated,

with a fan insuring thermal uniformity. Convection allows rapid homogenization of the air within the chamber, and the temperature is continually monitored by sensors attached to the LCVR mount.

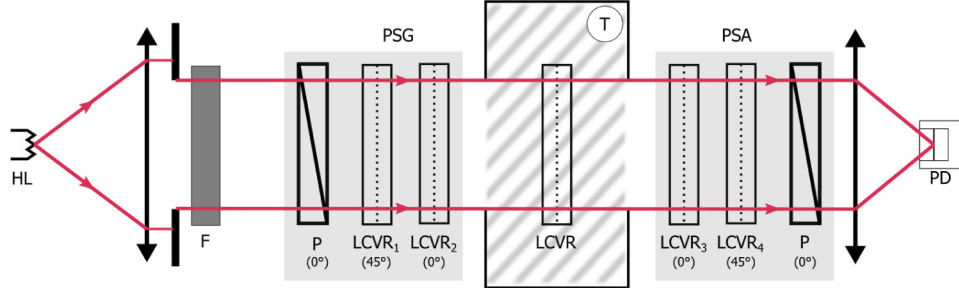


Fig. 3. Scheme of the optical setup for Experiment 1. HL: Halogen Lamp, F: dichroic filter, PSG: polarization state generator, PSA: polarization state analyzer, PD: Photo-diode. The hatched box represents the heated enclosure.

The polarimetric response of the LCVR is measured by means of a home-built Mueller polarimeter. The light source is a fiber-guided halogen lamp (Dolan-Jenner MI 150) with collimation (Avenir TV zoom lens 75mm, f/22) and a spectral filter for 600 nm (50 nm FWHM, Edmund Optics #84-797). A Polarization State Generator, consisting of a polarizer followed by two LCVRs, generates four illumination states. The light transmitted by the LCVR impinges on a Polarization State Analyzer (PSA), consisting of the same elements as the PSG in a reverse order. Behind the PSA, a lens ($f = 35\text{mm}$, Thorlabs) concentrates the outgoing light onto a single-channel silicon detector (PDA 100A2 Thorlabs).

After calibration [13], the polarimeter allows rapid measurement of the Mueller matrix $M(T, V)$ of the LCVR [14]. To obtain the retardance $\phi(T, V)$, the Mueller matrix is fitted with the Mueller matrix of an elliptic retarder :

$$\phi(T, V) = \arg \min_{\theta, \phi, \epsilon} (||M(T, V) - M_R^{\text{th}}(\theta, \phi, \epsilon)||_{\infty}). \quad (12)$$

Experiment 2 shares its main components with Experiment 1, as illustrated on Fig. 4. For this experiment, the liquid-crystal PSG behind the bandpass filter is replaced by a mechanical PSG. It consists of: a polarizer (Newport, 20LP-VIS), and a rotating waveplate ($\lambda/4$ at 632.8 nm, Newport, 20RP34). The waveplate generates a retardance of 96.4° at the operating wavelength (600 nm). The angular positions: -51.69° , -15.12° , 15.12° , 51.69° , permit to produce an optimized set of 4 distinct polarization states [15,16]. In this configuration, the measurement matrix W of the PSG has a condition number of $\kappa(W) = 3.07$. Compared to the liquid-crystal PSG, this modulator operates at much lower speeds but is stable over longer periods of time (e.g., against perturbations due to daytime temperature fluctuations in the laboratory). The PSA is removed from the experiments, and replaced by a single polarizer. The light source, the heated enclosure and the detector remain in place.

3.2. Characterization of a compensated module

In Experiment 2, two LCVRs are placed in front of the linear polarizer, on the detector side. They are oriented so as to have their fast axis (i) perpendicular to each other and (ii) forming a $\pm 45^\circ$ angle with the axis of the polarizer. Such a combination sets the LCM. The goal here is to find operating voltages V_A and V_B that would ensure temperature stable functioning.

The combination of the LCM and linear polarizer positioned before the detector acts as an elliptic polarizer. We note S its Stokes vector. For each measurement, the PSG generates 4 input

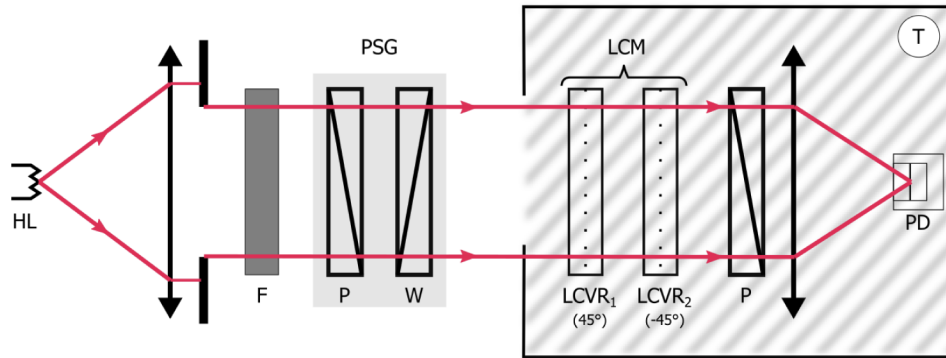


Fig. 4. Scheme of the optical setup for Experiments 2. HL: Halogen Lamp, F: dichroic filter, P: polarizer, W: rotating waveplate, PD: Photo-diode. The hatched box represents the heated enclosure.

Stokes vectors aggregated in a 4x4 matrix W . If we note I the 4-dimensional vector filled with intensity measurements after a full rotation of the waveplate, we obtain the following equation:

$$I = SW \quad (13)$$

which can be easily inverted so as to provide S .

On the Poincaré sphere, the effect of a retarder is equivalent to a rotation around the Stokes vector directed by its eigenaxis [17]. The angle of rotation is the retardance ϕ . The LCM acts as a waveplate with fixed axis and variable retardance. By varying the retardance, the resulting Stokes vector would describe a circle on the Poincaré Sphere. The axis of the LCM is as the normal to the plane containing such a circle. The retardance $\phi(T, V_A, V_B)$ of the LCM is obtained by computing the angle of the rotation transforming the Stokes vector of the polarizer ($S = [1, -1, 0, 0]^T$) into the measured Stokes vector.

4. Results

4.1. Characterization of the temperature-dependent retardance of a single LCVR

In order to test the model that has been introduced in section 2.1 (Eq. 5), Experiment 1 is used. The temperature inside the enclosure is raised to 45°C and, while the system thermalizes back to room temperature, the retardance $\phi(T, V)$ of the LCVR is measured every minute. For each temperature, a voltage scan is performed across a large portion of the LCVR operating range, with measurements made every 0.5V from 0.5 to 7V.

Figure 5(a) shows the retardance as a function of the applied voltage for two temperatures, towards the beginning (44°C) and the end (24°C) of the thermalization process. The shape of the curve remains the same: the retardance is highest at low voltage, it remains constant until a threshold is exceeded (Fréedericksz transition occurs at about 1.2V for this crystal), then the retardance decreases sharply at lower voltage and more slowly towards higher voltages. The relative difference between the curves may appear small considering the large temperature deviation: about 10% decrease has been observed over 20°C. However, the absolute difference in retardances may reach very high values (up to 50°).

The linearity of temperature dependent retardance is validated by observing its evolution for a given voltage, as illustrated in Fig. 5(b). Here we show the curves for two voltage points, at 2 V and at 5 V. The gap between the two selected curves being as large as $\approx 175^\circ$ at 20°C, we have subtracted the retardance at 20°C for a better visualization. Linear fits are represented with a

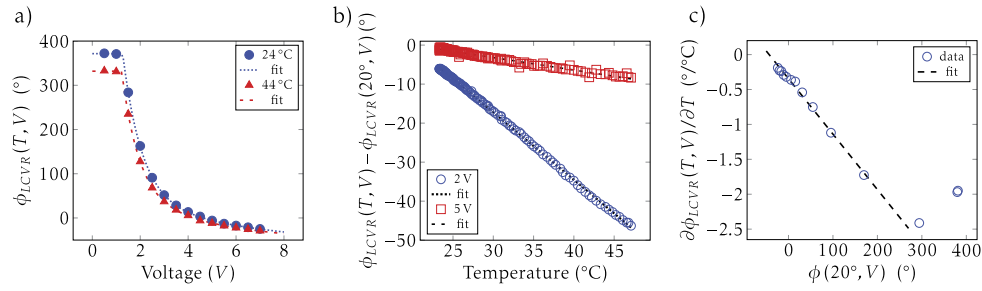


Fig. 5. Experimental validation of the temperature dependence of a single LCVR. a) retardance as a function of voltage at 24°C (blue points) and 44°C (red points). The dotted lines are a mere guide for the eyes. b) Evolution of retardance with temperature at fixed voltages: 2V (blue circles) and 5V (red squares). Dotted lines are linear fits of the experimental data. c) Slope of the temperature dependence of the retardance ($\partial\phi(T, V)/\partial T$) as a function of the retardance at 20°C ($\phi(20^\circ\text{C}, V)$). The dotted line is a linear fit of the data up to $\phi(20^\circ\text{C}, V) = 270^\circ$.

dotted line. Excellent agreement is obtained with the linear model (fit with $r^2 = 0.9994$ at 2 V and 0.9751 at 5 V) over the whole measured temperature range, spanning more than 20°C.

According to the model established in Eq. (5), the slope of $\phi(T)$ is proportional to the retardance at starting temperature T_0 . We note $\partial\phi(T, V)/\partial T$ the slopes fitted for each voltage, and $\phi(20^\circ\text{C}, V)$ the retardance of the LCVR for that same voltage. As shown in Fig. 5(c), a linear dependence of the slope is observed up to about 200°. We obtain excellent agreement with the proposed model in this range ($r^2 = 0.9927$). However, at about 300° ($V = 1.5\text{V}$), the measured curve starts to deviate from linear behavior. This happens in a region where the slope of $\phi(V)$ is steep, and still at a fair distance from the Fréedericksz transition. For voltages below the Fréedericksz threshold, the slope of $\phi(T)$ drops to lower magnitude, indicating that the behavior of the liquid crystal could have different regimes in the presence or in the absence of a voltage. We also note that the intercept of the linear curve is not 0. This does not conflict with the model since the LCVR is compensated: it is manufactured with an additional retarder to respond with zero retardance at voltage $\approx 4\text{V}$ (see Fig. 5(a)). Consequently, x-axis values in Fig. 5(c) are shifted towards the left hand side.

4.2. Temperature stable modulator

In this section, we are aiming to characterize an LCM and to focus on its working points, i.e. the pairs of voltages (V_A , V_B) that ensure temperature-stable operation. To that end, two LCVRs with mutually orthogonal axes, are inserted in the heated enclosure (setup of Experiment 2). Since the linear model has been validated for a single LCVR, the retardance of the LCM will be measured at two extreme temperatures only (22°C and 50°C). We then consider the difference in retardances for these temperatures by considering numerous voltage pairs, and determine the points that would minimize such a difference.

Voltage pairs are chosen so as to obtain regularly distributed retardances (with 10° steps) covering the range of both LCVRs. They will be extracted from the voltage dependent retardance curves that were previously measured using the method proposed in [18]. In this experiment, which involves long durations needed to carry out measurements for all voltages, we wait until a steady state is established in the heated enclosure, and the desired temperature remains stable. Figure 6(a) illustrates the evolution of Stokes vectors as ϕ_A (resp. ϕ_B) is scanned over the retardance range of LCVR_A (resp. LCVR_B) while ϕ_B (resp. ϕ_A) is kept constant at 0°. As expected, the measurements lie on a circle on the Poincaré sphere. Estimation of the orientation

based on the normal to the circle plane provides the value of 42° . This deviation of is about 3° as compared to the expected value (45°). It will be taken into account when retrieving retardances and should not affect the results.

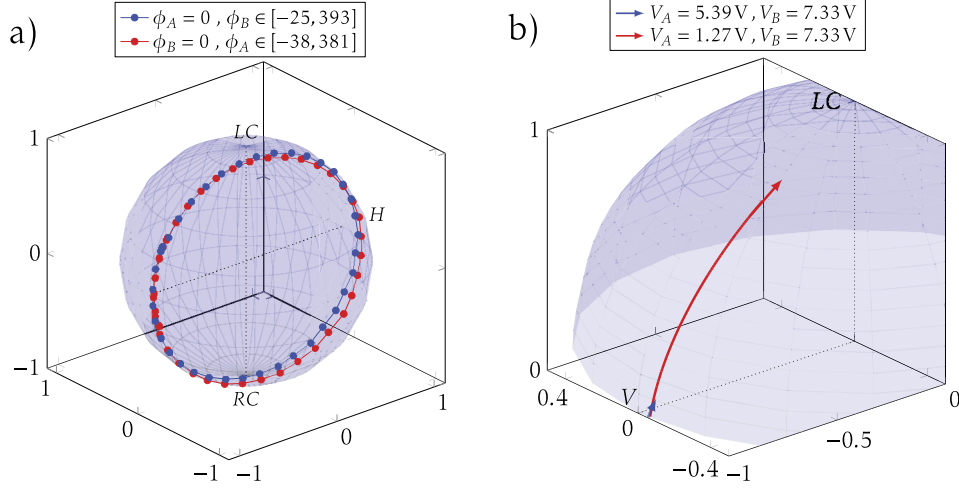


Fig. 6. Evolution of the measured Stokes vectors: a) with varying voltages at room temperature. Stokes vectors represented on the Poincaré sphere for: (blue line) ϕ_B scanning over the retardance range of LCVRB while $\phi_A = 0$, (red line) ϕ_A scanning over the retardance range of LCVRA while $\phi_B = 0$. b) with varying temperature between 22°C and 50°C : (blue lines) for $V_A = 5.39\text{V}$, $V_B = 7.33\text{V}$, (red lines) for $V_A = 1.27\text{V}$, $V_B = 7.33\text{V}$.

Figure 6(a) also shows that a same Stokes vector can be reached with different combinations of V_A and V_B . In general, a single ϕ_{LCM} can be obtained with a whole range of continuously varying ϕ_A and ϕ_B . However, depending on the temperature, ϕ_{LCM} might take very different values for a chosen voltage. This is illustrated in Fig. 6(b) for two voltage pairs corresponding to $\phi_{LCM} = 0$ at 22°C . In the first case, we choose ($V_A = 5.39\text{ V}$, $V_B = 7.33\text{ V}$), represented by the blue lines. ϕ_{LCM} remains stable with temperature, featuring a total variation of 4° retardance over a 28°C temperature range. The second case, with ($V_A = 1.27\text{ V}$, $V_B = 7.33\text{ V}$) is represented by red lines. Here, the LCM drifts significantly with temperature, and a variation of 65° is measured between 22°C and 50°C .

The total drift in retardance, noted $\Delta\phi_{LCM}$, is calculated as:

$$\Delta\phi_{LCM} = \phi_{LCM,50^\circ\text{C}} - \phi_{LCM,22^\circ\text{C}} = (\phi_{A,50^\circ\text{C}} - \phi_{B,50^\circ\text{C}}) - (\phi_{A,22^\circ\text{C}} - \phi_{B,22^\circ\text{C}}) \quad (14)$$

where $\phi_{module,T}$ is the retardance of the module (the LCM, LCVRA or LCVRB) at temperature T (22°C or 50°C). Figure 7(a) shows $\Delta\phi_{LCM}$ as a function of the retardance of LCVRA and LCVRB at 22°C for all considered voltage pairs. According to the model (Eq. (5)), $\Delta\phi_{LCM}$ should depend linearly on both $\phi_{A,22^\circ\text{C}}$ and $\phi_{B,22^\circ\text{C}}$. However, due to the discrepancy observed for high retardances, (see previous section), data points with initial retardances above 265° were excluded before fitting. For data points below such a threshold, the fitted surface is represented as a gray plane in Fig. 7(a). A good agreement with the model is obtained ($r^2 = 0.9857$). From the fit, the characteristic coefficient α of the LCVR was deduced: $\alpha_A = -0.84\%$ per $^\circ\text{C}$ and $\alpha_B = -0.43\%$ per $^\circ\text{C}$.

When drift-free operation is achieved, ϕ_{LCM} is independent of the temperature. The locus of such points in the 3D space of Fig. 7(a) is the horizontal plane of equation $\Delta\phi_{LCM} = 0$. It is represented as a purple plane in the figure. The location of the working points for a temperature

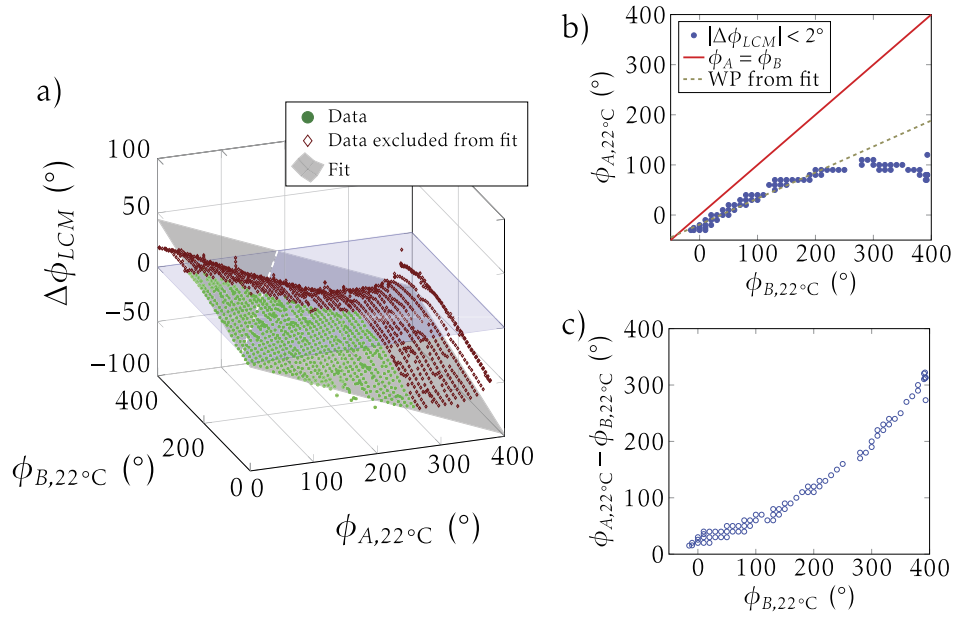


Fig. 7. LCM working points. a) Total drift in retardance of the LCM between 22°C and 50°C as a function of the initial retardance of LCVRA and LCVRB at 22°C. According to the model, the data can be fitted with a plane, represented in gray. Temperature stable points are in the plane of equation ($\Delta\phi_{LCM}=0$) represented in purple. b) ϕ_A at 22°C as a function of ϕ_B at 22°C for stable points ($\Delta\phi_{LCM}$ less than 2°). The dotted line is the intersection of the gray and purple planes from a). The red line indicates points with $\phi_{LCM}=0$ ($\phi_A = \phi_B$). c) ϕ_{LCM} as a function of $\phi_{B,22^\circ C}$. Note that $\phi_{LCM} = \phi_{A,22^\circ C} - \phi_{B,22^\circ C}$ can also be read graphically on a) as the distance of the working points to the red line.

stable LCM is hence given by the intersection of the surface representing $\Delta\phi_{LCM}$ with the purple plane. The working points predicted by the model are placed along the white dotted line, intersection of the gray and purple planes.

Points within 2° of deviation from the ($\Delta\phi_{LCM} = 0$)-plane are shown in Fig. 7(b), representing the empirical relationship between ϕ_A and ϕ_B for the LCM working points. On the same graph, the dotted gray line represents the relation derived from the model (see Eq. (10)). We observe that the working points diverge from the linear model as $\phi_{B,20^\circ C} > 200^\circ$.

However, such a deviation increases the range of stable retardances for the LCM, as shown in Fig. 7(c). Indeed, the resulting ϕ_{LCM} can be read graphically by measuring along the vertical direction, the distance between the empirical working points and the $\phi_A = \phi_B$ line. In our case, ϕ_{LCM} up to 250° can be obtained with $\phi_A = 100^\circ$ and $\phi_B = 350^\circ$.

5. Discussion and conclusion

We have proposed and thoroughly investigated on a new design for temperature-stable liquid crystal polarization modulators. The latter have been built by combining two LCVRs and by choosing suitable driving voltage. Based on a phenomenological and linear model of LCVR retardance, we have shown that an efficient compensation of temperature drift over a large retardance range is feasible. We have exposed the validity and the limits of the proposed model. Namely, we have observed, on the one hand, a linear dependence of retardance $\phi(T)$ with temperature over a large range and, on the other hand, the coefficient τ as in Eq. (5) is proportional to the retardance at the starting temperature T_0 . We have built an LCM by combining two

commercially available LCVRs and exhibited working points for temperature-stable operation. The mounted LCM has a working range of 22°C–50°C for temperature and, 250° of attainable retardance. Over these ranges, the retardance of the LCM remains constant within 2°. This is to be compared to drifts in excess of 50° observed for LCVRs over the same temperature range.

The working principle of LCMs is based on the validity of the linear model. More precisely, once the working point set, the retardance of both LCVRs must evolve identically. Based on the Haller formula and on low values of exponent β , the first-order approximation is expected to be valid over the temperature range that has been explored in this paper. Wider temperature ranges could be expected farther away from the critical point or, equivalently, by designing LCVRs with higher T_C .

Future work will focus on remaining unwanted effects affecting LCVRs (e.g., wavelength dependence, depolarization due to thermal agitation, polarization inhomogeneity etc.) and how the LCM design affects them. Our study also raises the question on how the retardance evolves with temperature, as a voltage is applied to the liquid crystals of the LCVRs. To the best of our knowledge, such an issue has not been explored. For example, the linear behavior of the slope observed in this study is a remarkable property that is yet to be understood.

Finally, the choice of the two LCVRs to construct the LCM is important. For a device that would operate over a wide retardance range, the LCVRs should ideally have wide retardance ranges themselves and α values as different as possible. Such an optimized LCM could be obtained either by carefully choosing LCVRs among existing ones or, again, by chemical engineering of new liquid crystal mixtures.

In the proposed design, the LCM acts as a temperature stable LCVR and can be used in any LCVR-based polarimeter. It corrects one of the main drawbacks of LCVRs while preserving their advantages. These features should open up new perspectives, particularly for polarimeters operating in demanding environments, such as bio-medical or space-based measurements.

Funding. Société d'Accélération du Transfert de Technologies (Conectus Alsace, Dermapol project).

Acknowledgments. The authors are grateful to the anonymous reviewers for their fruitful comments.

Disclosures. JZ, MT and CH declare a patent (P). JR, JD, BV and YT declare no conflicts of interest.

Data availability. Data underlying the results presented in this paper are not publicly available at this time but may be obtained from the authors upon reasonable request.

Supplemental document. See [Supplement 1](#) for supporting content.

References

1. D. H. Goldstein and R. A. Chipman, "Error analysis of a Mueller matrix polarimeter," *J. Opt. Soc. Am. A* **7**(4), 693 (1990).
2. J. Li, S. Gauza, and S. T. Wu, "Temperature effect on liquid crystal refractive indices," *J. Appl. Phys.* **96**(1), 19–24 (2004).
3. A. R. Tiwary, A. Raja Bayanna, and S. K. Mathew, "Estimation of order parameter of a liquid crystal variable retarder using Haller's approximation," *Appl. Opt.* **56**(14), 4180 (2017).
4. J. C. Gladish and D. D. Duncan, "Alignment and temperature effects in liquid-crystal-based active polarimetry," *Appl. Opt.* **53**(18), 3982 (2014).
5. C. V. Brown, "Physical properties of nematic liquid crystals," *Handbook of Visual Display Technology* (Springer International Publishing, 2016), pp. 1953–1975.
6. P.-G. De Gennes and J. Prost, *The physics of liquid crystals*, 83 (Oxford university press, 1993).
7. I. Haller, "Thermodynamic and static properties of liquid crystals," *Prog. Solid State Chem.* **10**, 103–118 (1975).
8. E. G. Hanson and Y. R. Shen, "Refractive Indices and Optical Anisotropy of Homologous Liquid Crystals," *Mol. Cryst. Liq. Cryst.* **36**(3–4), 193–207 (1976).
9. R. L. Heredero, N. Uribe-Patarroyo, T. Belenguer, G. Ramos, A. Sánchez, M. Reina, V. Martínez Pillet, and A. Álvarez-Herrero, "Liquid-crystal variable retarders for aerospace polarimetry applications," *Appl. Opt.* **46**(5), 689–698 (2007).
10. P. García Parejo and A. Álvarez-Herrero, "Liquid crystals for space instrumentation: optical properties of liquid crystal mixtures for polarimeters," *Opt. Mater. Express* **9**(6), 2681 (2019).
11. S. R. Johnson and P. C. Jurs, "Prediction of the Clearing Temperatures of a Series of Liquid Crystals from Molecular Structure," *Chem. Mater.* **11**(4), 1007–1023 (1999).

12. J. Zallat, M. Torzynski, A. Lallement, and C. Heinrich, "Device for compensating for the drift of a phase shift of a device for modulating the polarization state of a light beam," U.S. patent US20160139033A1 (19 May 2016).
13. E. Compain, S. Poirier, and B. Drevillon, "General and self-consistent method for the calibration of polarization modulators, polarimeters, and Mueller-matrix ellipsometers," *Appl. Opt.* **38**(16), 3490 (1999).
14. A. De Martino, Y.-K. Kim, E. Garcia-Caurel, B. Laude, and B. Drévillon, "Optimized Mueller polarimeter with liquid crystals," *Opt. Lett.* **28**(8), 616 (2003).
15. A. Ambirajan and D. C. L. Jr., "Optimum angles for a polarimeter: part I," *Opt. Eng.* **34**(6), 1651–1655 (1995).
16. J. Zallat, S. Aïnouz, and M. P. Stoll, "Optimal configurations for imaging polarimeters: Impact of image noise and systematic errors," *J. Opt. A: Pure Appl. Opt.* **8**(9), 807–814 (2006).
17. D. H. Goldstein, *Polarized Light* (CRC Press, 2017).
18. J. M. López-Téllez and N. C. Bruce, "Stokes polarimetry using analysis of the nonlinear voltage-retardance relationship for liquid-crystal variable retarders," *Rev. Sci. Instrum.* **85**(3), 033104 (2014).